

THE ABSENCE OF CRYSTALLINE SILICATES IN THE DIFFUSE INTERSTELLAR MEDIUM¹

F. KEMPER,^{2,3} W. J. VRIEND,⁴ AND A. G. G. M. TIELENS^{4,5}

Received 2003 November 27; accepted 2004 March 11

ABSTRACT

Infrared spectroscopy provides a direct handle on the composition and structure of interstellar dust. We have studied the dust along the line of sight toward the Galactic center using Short Wavelength Spectrometer data obtained with the *Infrared Space Observatory (ISO)*. We focused on the wavelength region from 8 to 13 μm , which is dominated by the strong silicate absorption feature. Using the absorption profiles observed toward Galactic center sources 3 and 4, which are C-rich Wolf-Rayet Stars, as reference objects, we are able to disentangle the interstellar silicate absorption and the silicate emission intrinsic to the source, toward Sgr A* and derive a very accurate profile for the intrinsic 9.7 μm band. The interstellar absorption band is smooth and featureless and is well reproduced using a mixture of 15.1% amorphous pyroxene and 84.9% of amorphous olivine by mass, all in spherical submicron-sized grains. There is no direct evidence for substructure due to interstellar crystalline silicates. By minimizing χ^2 of spectral fits to the absorption feature, we are able to determine an upper limit to the degree of crystallinity of silicates in the diffuse interstellar medium (ISM) and conclude that the crystalline fraction of the interstellar silicates is $0.2\% \pm 0.2\%$ by mass. This is much lower than the degree of crystallinity observed in silicates in the circumstellar environment of evolved stars, the main contributors of dust to the ISM. There are two possible explanations for this discrepancy. First, an amorphization process occurs in the ISM on a timescale significantly shorter than the destruction timescale, possibly caused by particle bombardment by heavyweight ions. Second, we consider the possibility that the crystalline silicates in stellar ejecta are diluted by an additional source of amorphous silicates, in particular supernovae. We also compare our results with a study on silicate presolar grains found in interplanetary dust particles.

Subject headings: astrochemistry — cosmic rays — dust, extinction — Galaxy: center — infrared: ISM — ISM: lines and bands

1. INTRODUCTION

In the last decade, a multitude of evidence for the presence of crystalline silicates in various astrophysical environments has emerged. In particular, infrared spectra have revealed that silicates in circumstellar environments often contain a significant crystalline fraction around both post-main-sequence stars (e.g., Waters et al. 1996; Molster et al. 2002) and pre-main-sequence stars (e.g., Waelkens et al. 1996; Meeus et al. 2001). In addition, crystalline silicates are ubiquitous in the solar system, not only in the more evolved bodies such as planets, but also in primitive objects like comets (e.g., Wooden 2002). Because crystallization is inhibited by high-energy barriers, the origin and evolution of the crystalline silicate fraction in interstellar and circumstellar media has the potential to provide direct evidence of the energetic processing of grains.

The life cycle of dust starts in the outflow of evolved stars, continues upon ejection in the interstellar medium (ISM), and eventually ends in the planet-forming disk around a young star. It is surprising that, whereas crystallinity is prevalent at the beginning and end of dust grains' lives, no crystallinity is

found in the intermediate phase (i.e., in the diffuse ISM). In fact, a relatively high upper limit to the degree of crystallinity in the diffuse ISM has been determined recently (Li & Draine 2001). Less than 5% by number of the interstellar Si atoms were found to be incorporated in crystalline silicate grains of less than 1 μm in size, which is roughly equivalent to a mass fraction of less than 5%. On the other hand, Bowey & Adamson (2002) have suggested that while the broad and structureless interstellar 10 μm absorption feature is commonly ascribed to amorphous silicates, the crystalline spectral detail may be washed out in a very complex mixture of crystalline silicates. Furthermore, some studies on silicates in the dense ISM have reported the (controversial) detection of crystalline silicate features (Cesarsky et al. 2000; Onaka & Okada 2003), but one has to bear in mind that this environment has physical properties very different from those of the diffuse ISM.

In this work, we readdress the issue of crystallinity in the diffuse ISM by studying the line of sight toward the Galactic center (GC). Because of its large amount of extinction and its high infrared flux, the sight line toward the GC has often been used to characterize the properties of interstellar dust (Roche & Aitken 1985; Rieke et al. 1989; Pendleton et al. 1994; Tielens et al. 1996; Lutz et al. 1996; Chiar et al. 1998). We study the 10 μm silicate absorption feature in order to determine the degree of crystallinity in this line of sight. In § 2 we discuss the *Infrared Space Observatory (ISO)* Short Wavelength Spectrometer (SWS) observations and data reduction, as well as the characteristics of the region around Sgr A* and the correction method applied for emission intrinsic to the GC region. The method used to determine the dust composition in the diffuse ISM is described in § 3, along with the results.

¹ Based on observations with *ISO*, an ESA project with instruments funded by ESA Member States (especially the PI countries: France, Germany, the Netherlands and the United Kingdom) and with the participation of ISAS and NASA.

² Department of Physics and Astronomy, UCLA, 405 Hilgard Avenue, Los Angeles, CA 90095-1562; kemper@astro.ucla.edu.

³ Spitzer Fellow.

⁴ Kapteijn Institute, University of Groningen, P.O. Box 800, 9700 AV Groningen, Netherlands.

⁵ SRON Laboratory for Space Research, P.O. Box 800, 9700 AV Groningen, Netherlands.

TABLE 1
DETAILS OF THE *ISO* SWS OBSERVATIONS

Object	α (J2000)	δ (J2000)	AOT	Speed	t_{int} (s)	Observation Date
Sgr A*	17 45 40.0	-29 00 29	1	4	6528	1996 Feb 19
GCS 3	17 46 14.8	-28 49 34	1	3	3454	1996 Aug 29
GCS 4	17 46 15.7	-28 49 47	1	3	3454	1996 Sep 8

NOTE.—Units of right ascension are hours, minutes, and seconds, and units of declination are degrees, arcminutes, and arcseconds.

In § 4 we discuss two mechanisms to explain the discrepancy in crystallinity observed between stellar ejecta and the diffuse ISM. A comparison with silicates in the solar system and planet-forming disks around other stars is given in § 5. Section 6 contains the conclusions.

2. OBSERVATIONS AND DATA REDUCTION

2.1. *ISO* SWS Observations of Sgr A* and Nearby Objects

During the lifetime of the *ISO* mission (Kessler et al. 1996), 2.38–45.2 μm SWS spectra (de Graauw et al. 1996) of the GC and two sight lines in the nearby Quintuplet cluster were obtained. Table 1 gives an overview of these observations.

The GC region is very crowded, while the beam *ISO* used for the SWS observations is very large. In Figure 1 the orientation and positions of the beam is indicated on a 12.4 μm map of the GC (Tanner et al. 2002). The beam includes infrared sources (IRS) 1, 2, 3, 7, 9 and 10, of which IRS 1 is the brightest at 12.4 μm . At the position of Sgr A* itself there is virtually no 12.4 μm emission. IRS sources 1, 2, 9, and 10 lie along an arc on the so-called Ridge, generally believed to be a complex of H II regions. IRS 7 is a late-type supergiant and is the brightest 2.2 μm source in the vicinity of the GC. IRS 3, an OH/IR star, shows the 10 μm silicate feature in absorption (Becklin et al. 1978). In the large SWS beam, the mid-IR emission is dominated by the extended emission associated with IRS 1.

Galactic center sources (GCSs) 3 and 4 are members of the Quintuplet cluster. The positions of the beams are indicated on the ISOCAM image presented in Figure 1 of the study by Moneti et al. (2001). In the observation of GCS 3, the beam was centered on GCS 3-I (or Q4); however, GCS 3-II (or Q2) is the brightest mid-infrared source in the beam and dominates the measured spectrum (Moneti et al. 2001).

2.2. Data Reduction

The full *ISO* SWS spectrum of the line of sight toward the GC was first published by Lutz et al. (1996). We chose to reduce this spectrum again to fully address the problems caused by the detector memory effects in band 2. In addition, we used the SWS spectra of GCS 3 and 4 as a reference to correct for the silicate emission intrinsic to the Sgr A* region. The spectra of GCS 3 and 4 were previously published in the aforementioned work by Moneti et al. (2001), but we re-did the data reduction to be consistent with the reduction of the spectrum of Sgr A*.

We used the Interactive Analysis package (IA³) to reduce all three spectra. In addition to the automated routines provided in this package, the up and down scans were analyzed separately to remove glitches and detector jumps by hand. To correct for the detector memory effects, most prominently present in band 2 (ranging from 4.08 to 12.0 μm), the Fouks-Schubert

model was applied (see § 2.3). From the spectra in band 2c and all subbands of band 3 (ranging from 7.00 to 29.0 μm) we removed residual fringes that were present after the relative spectral responsivity function was applied. Rebinning according to actual spectral resolution was performed ($R = 1000$ for the speed 4 observations of Sgr A* and $R = 500$ for the speed 3 spectra of GCS 3 and 4), and data points deviating more than 3σ per bin were removed, resulting in a loss of 2% of the data points. Narrow spectral lines were excluded from sigma clipping. Finally, the spectra from the individual detectors were rescaled to the average flux levels to produce a smooth spectrum rather than a dot cloud.

2.3. Detector Memory Effects

It is known that *ISO* SWS spectroscopy suffers from memory effects in the data, a problem predominantly found in data from bands 2 and 4 (i.e., the wavelength ranges from 4.08 to 12.0 μm and 29.0 to 45.2 μm). The semiconductors that the detectors consist of do not fully discharge between subsequent measurements in a wavelength scan. When the flux levels in a

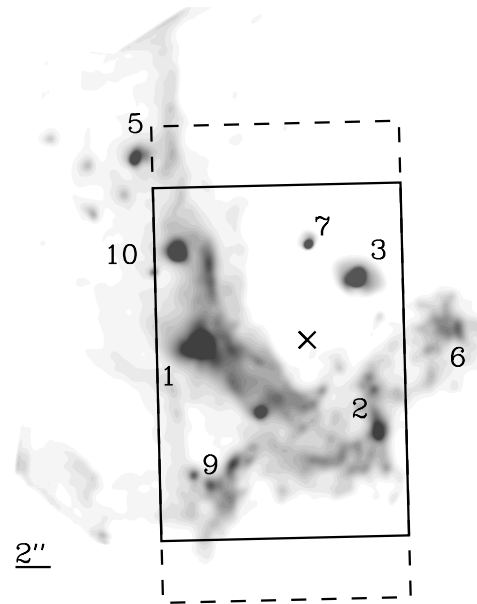


FIG. 1.—Position of the *ISO* SWS beam toward the GC. This plot shows a map of the GC at 12.4 μm (Tanner et al. 2002), on which we overplotted the pointing of *ISO* SWS. The position of Sgr A* is indicated with a cross, and the numbers indicate the positions of the GC IRS sources, following the notation from Becklin et al. (1978). The beam for the SWS detectors working at $12.0 < \lambda \leq 27.5 \mu\text{m}$ is indicated with a solid line. The dashed line indicates the beam size when observing at $12.0 < \lambda \leq 27.5 \mu\text{m}$. The beam includes infrared sources 1, 2, 3, 7, 9, and 10. For an image showing the two *ISO* SWS beam positions toward the Quintuplet sources, the reader is referred to Fig. 1 of Moneti et al. (2001).

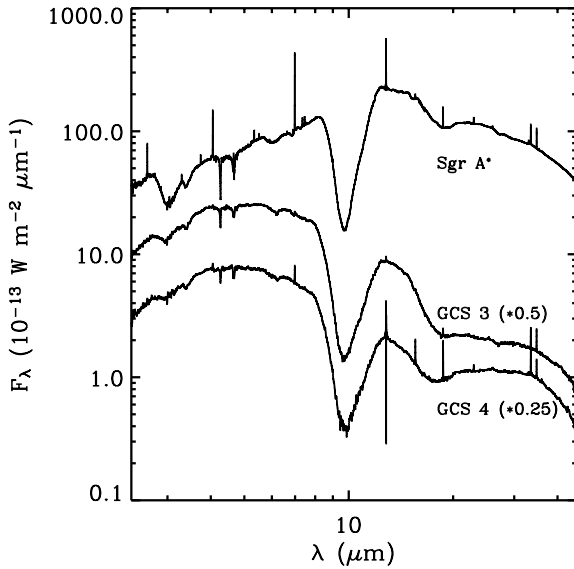


FIG. 2.—The 2.38–45.2 μm *ISO* SWS spectra of Sgr A*, GCS 3, and GCS 4. To enhance the clarity of the figure, the flux levels of GCS 3 and GCS 4 are multiplied with a factor of 0.5 and 0.25, respectively.

certain (sub)band vary only by a small amount, this is not a large problem, since the amount of memory in each measurement will be more or less constant, and simply generates an offset in the flux levels. The relative flux levels will not be affected, so it may be relatively easy to correct for the memory when subtracting the *dark current*. In cases in which a large variation in flux levels occurs within one subband, the memory effects require additional attention. This is the case in band 2c, ranging from 7.00 to 12.0 μm , which contains the entire interstellar absorption feature due to silicates. The discharging of the semiconducting material can be described with a set of differential equations (Fouks & Schubert 1995). This model expresses the time delay in the charging on the incident intensity. The larger the change in flux levels, the longer it takes to reach the charging corresponding to the incident flux. Vriend (1999) has applied the Fouks-Schubert model to the data in band 2 and was able to correct for the memory effects. The successful application of this model can be easily checked by comparing the data of the up- and down-scans separately, since the memory effects should affect these data in opposite wavelength directions. This difference is minimized when the memory correction is applied successfully. Only a very small residual memory effect remains. The application of the Fouks-Schubert model to correct for memory effects in band two, which was first developed for the data analysis of the GC line of sight (Vriend 1999), is now implemented in the IA³ package and the *ISO* standard pipe line data products (Leech et al. 2003; Kester 2003).

2.4. Correction for Silicate Emission Intrinsic to Sgr A*

Figure 2 shows the *ISO* SWS spectra of Sgr A*, GCS 3 and GCS 4. Since it is thought that the absorption feature at 10 μm is caused by interstellar dust particles along the line of sight, and that the dust composition along those lines of sight is very similar, it is remarkable that the 10 μm absorption feature toward Sgr A* seems to be much narrower than the features observed toward the Quintuplet stars. This is illustrated in Figure 3b, which gives the raw optical depth τ_{raw} for GCS 3 and Sgr A* calculated directly from $F_{\nu, \text{obs}} = F_{\nu, 0} e^{-\tau_{\text{raw}}}$, where

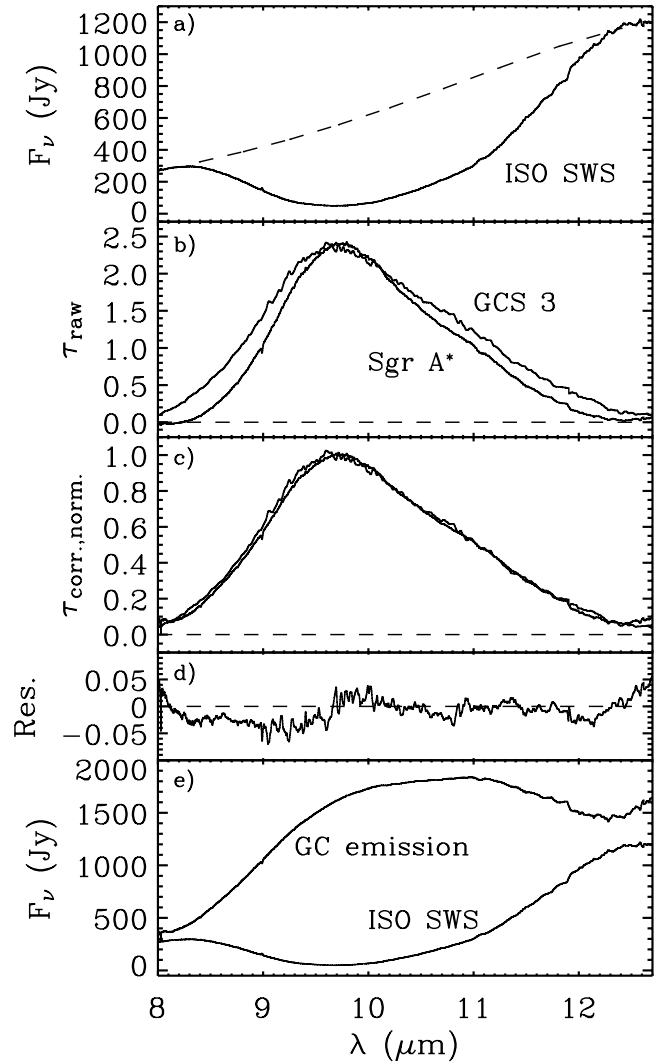


FIG. 3.—Steps in the data reduction process. (a) The observed spectrum of the Sgr A* region, along with a fourth-order polynomial continuum (*dashed line*). (b) The raw optical depth in the 10 μm feature in Sgr A* and GCS 3. (c) The Sgr A* absorption feature is corrected for emission intrinsic to the GC and now nicely overlaps with the optical depth toward GCS 3. Both spectra are normalized. The remaining difference between the two normalized optical depths is shown in (d). Finally, (e) shows what the intrinsic emission from the GC region would have looked like if there were no interstellar silicate absorption. This part of the spectrum is only de-reddened for optical depth *in* the silicate feature; however, this feature is of course superposed on a continuum of extinction, giving rise to ~ 30 mag of extinction in the optical.

$F_{\nu, 0}$ is a continuum determined using fourth-order polynomial fitting.

The stars in the Quintuplet cluster are identified as carbon-rich Wolf-Rayet stars (Figer et al. 1999). We therefore assume that there are no circumstellar silicates that give rise to emission or absorption features intrinsic to the Quintuplet stars and that the shape of the feature is entirely determined by interstellar absorption. Indeed, Moneti et al. (2001) conclude that the Quintuplet cluster does not contain any gas or dust between its stellar components and that the silicate absorption feature is a truly interstellar feature.

We assume that the dust composition in the line of sight toward Sgr A* does not differ much from that toward the Quintuplet sources, and we therefore conclude that the difference of the absorption profile can be explained by silicate emission intrinsic to the Sgr A* region. It has been reported

that the line of sight toward the GC contains more molecular clouds than those toward the Quintuplet sources (Chiar et al. 2001). We assume that this only leads to a difference in optical depth and not to a difference in dust composition. Rather, we attribute the difference in the $10\ \mu\text{m}$ profile of Sgr A* and the Quintuplet sources to the presence of underlying silicate emission in the former. Since the signal-to-noise ratio of the spectrum observed toward Sgr A* is much better than that of the data of the Quintuplet source, we are aiming to correct for the silicate emission local to Sgr A* to obtain the intrinsic interstellar profile. We assume that the silicate contribution local to Sgr A* gives rise to the same feature in emission as it does in absorption. Likely, the silicate emission is associated with dust in the H II region, IRS 1. Because the resulting observed absorption feature is determined by the intrinsic emission and interstellar absorption, we applied an iterative process to determine the shape of the interstellar absorption and GC emission feature. The differences with GCS 3 or GCS 4 are minimized (the best results are achieved for GCS 3; see Figs. 3c and 3d), finally resulting in the corrected interstellar absorption feature. Figure 3e shows the spectral appearance of the GC silicate emission feature; the reader must keep in mind that first, the emission is the sum of all the mid-infrared sources in the *ISO* beam, and second, the spectrum is only de-reddened for the optical depth *in* the feature and that the fact that the silicate interstellar absorption feature is superposed on an extinction continuum is ignored.

A similar correction to determine the interstellar absorption in the $10\ \mu\text{m}$ feature was first performed by Roche & Aitken (1985), who used the silicate profile of red supergiant μ Cep as a template for the interstellar absorption in order to de-redden their observations of the GC environment. This was justified by the resemblance between the μ Cep silicate feature and the absorption feature observed toward a number of carbon-rich Wolf-Rayet stars (Roche & Aitken 1984).

3. DETERMINATION OF THE DUST COMPOSITION

3.1. Method

The corrected optical depth τ is presented in Figures 3c and 4 and can be compared directly to the opacity of the various dust components at these wavelengths. The mass absorption coefficient κ correlates to the optical depth according to $\tau_\lambda = \rho_d \kappa_\lambda L = n m_d \kappa_\lambda L$, where L is the distance to the GC, ρ_d is the average density of the considered dust species, n is the number density of grains, and m_d is the average mass of a dust grain. We can define the mass column density $N_i = \rho_{d,i} L$ and thus fit the $10\ \mu\text{m}$ absorption feature by solving

$$\tau_\lambda = \sum_i N_i \kappa_{\lambda,i} \quad (1)$$

for N_i . A continuum subtraction is performed on the mass absorption coefficients between the same wavelength boundaries that were used to obtain the optical depth in the interstellar $10\ \mu\text{m}$ feature. Consequently, only the contribution to the optical depth in features is taken into account.

In order to solve equation (1), we applied the χ^2 fitting method, which involves minimizing

$$\chi^2 = \sum_\lambda \left(\frac{\tau_\lambda - \sum_i N_i \kappa_{\lambda,i}}{\sigma_\lambda} \right)^2, \quad (2)$$

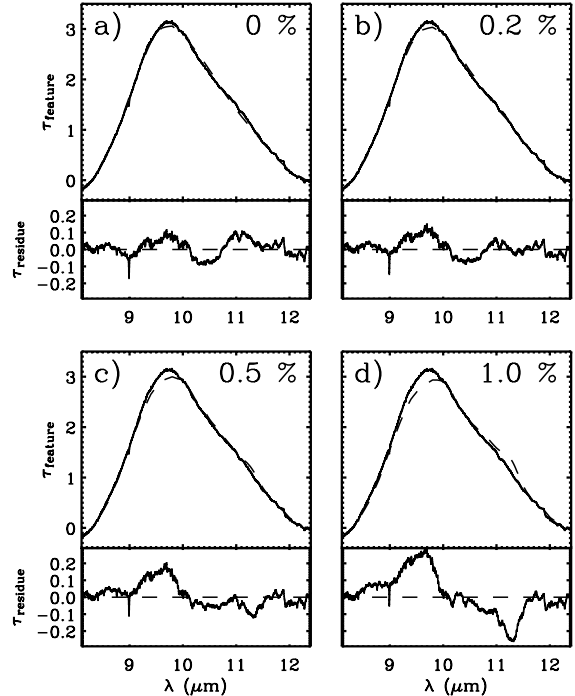


FIG. 4.—Optical depth observed in the $10\ \mu\text{m}$ silicate feature toward Sgr A*. (a) The best χ^2 fit consisting of a mixture of amorphous silicates (*dashed line*) to the optical depth in the feature (*solid line*). The lower part of (a) shows the residual optical depth after the fit is subtracted from the observed optical depth. (b–d) The best χ^2 fit (*dashed line*) to the *ISO* data (*solid line*) of partially crystalline mixtures of silicates with the same ratio of pyroxenes over olivines as in (a). In each panel the degree of crystallinity is indicated in the upper right corner, and the lower part of each panel shows the residual optical depth. In the case of the completely amorphous dust composition, the residuals are at most $\sim 3\%$ of the optical depth of the amorphous silicates. The χ^2 values are smallest for the 0.2% degree of crystallinity, which is evident from the residuals as well. With increasing crystallinity, the fit quickly deteriorates, which becomes visible as larger residuals. At $\sim 0.5\%$, the fit is already worse than a completely amorphous composition.

where σ_λ is the uncertainty in the measured values arising from our data reduction procedure. They represent the spread in individual measurements of the 12 different SWS detectors, before the spectrum was collapsed into 1 point per spectral bin. A measure for the goodness of fit is given by the reduced χ^2 value, χ^2_ν , defined as $\chi^2_\nu = \chi^2/\nu$ with $\nu = N_p - m$. The parameter N_p represents the number of data points in the spectrum, and m gives the number of free parameters. The χ^2_ν values derived by our fitting method can be very high (at least ~ 44), while textbook examples always require this value to be close to unity. Two different effects contribute to these high values.

First, σ_λ is only determined by the random scatter in the measurements, while the systematic errors in the flux levels can be significantly higher than that. Sources for these systematic errors could be residuals of the memory effect, which can be as high as 2% in either direction or features introduced by the responsivity functions. Second, the application of a χ^2 fitting method assumes that the model does not contain uncertainties. In fact, the model spectra we use are based on mass absorption coefficients measured in the laboratory and therefore have intrinsic uncertainties. It is hard to quantify the combined effect of the uncertainties in the laboratory spectra and the systematic errors in the *ISO* SWS data. We have elected to use only the uncertainties directly resulting from the *ISO* SWS data in the χ^2 fitting method.

We performed fits with different dust components, both amorphous and crystalline silicates. First, we have determined confidence levels for the fit with only amorphous dust components (see § 3.2) using the method discussed by Press et al. (1992). In addition we use the F -test (Bevington & Robinson 1992) to determine the goodness of the fits when crystalline silicates were added. This test shows how much a χ^2 fit improves if a parameter is added. The value F_χ is calculated from

$$F_\chi = \frac{\Delta\chi^2}{\chi_v^2}, \quad (3)$$

where $\Delta\chi^2$ is the decrease in χ^2 between the initial and new fit, and χ_v^2 is the value from the fit with the extra parameter added (i.e., the new fit). The parameter F measures the relative improvement of the χ^2 of a fit to randomly scattered data when an additional component is included. The larger the value of F , the more significant is the improvement (see, e.g., Bevington & Robinson 1992, p. 209).

3.2. The Amorphous Component

In order to find the mass fraction contained in the crystalline silicates, the total mass in the amorphous component has to be determined, which depends on its composition. The chemical composition of amorphous silicates is determined by the formation path. Amorphous silicates resulting from the amorphization of crystalline silicates will have the stoichiometry of that crystal, while amorphous silicates formed through direct condensation from a gas cloud or by collisions and subsequent merging of two distinct grains are most likely to have a non-stoichiometric composition. Most measurements of the optical properties of amorphous silicates are limited to the stoichiometries of olivines and pyroxenes, except for a recent study by Jäger et al. (2003a), who applied the sol-gel method to construct amorphous silicates of some selected non-stoichiometric compositions. In the sol-gel method, Mg- and Si-hydroxides [$\text{Mg}(\text{OH})_2$ and $\text{Si}(\text{OH})_4$] are mixed in the liquid phase. Extraction of H_2O by chemical reaction between the Mg- and Si-hydroxides then gives rise to the formation of silicates. Because the two components can be mixed in any desired ratio, it is possible to synthesize non-stoichiometric amorphous Mg-silicates. For more details, the reader is referred to the work by Jäger et al. (2003a). However, the spectral appearance of these materials does not match the interstellar absorption feature, therefore we only consider stoichiometric compositions. We have used the optical constants determined by Dorschner et al. (1995) for olivine (MgFeSiO_4) and pyroxene ($\text{MgFeSi}_2\text{O}_6$). The use of laboratory optical constants allows us to immediately convert the derived optical depths into column densities of dust as well as derive their chemical composition.

The appearance of the $10 \mu\text{m}$ feature depends on the grain shape and grain size of the silicate particles. In Figure 5 an overview of the most important effects is given for both amorphous olivine and pyroxene. Small spherical grains (up to $\sim 0.1 \mu\text{m}$ in size) all produce exactly the same shape for the spectral feature. For larger grains, the feature starts to broaden toward longer wavelengths. This effect becomes stronger with increasing grain size. The use of nonspherical grains, represented by a continuous distribution of ellipsoids (CDE; Bohren & Huffman 1983), tends to shift the peak of the feature to longer wavelengths. With CDE calculations it is impossible to include any information on grain size. Amorphous olivine, in

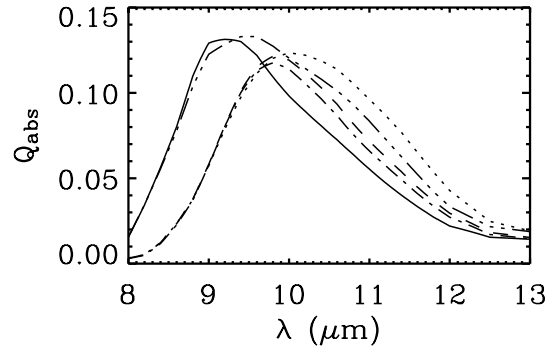


FIG. 5.—Absorption efficiencies of amorphous silicates in the 8–13 μm range, calculated from optical constants provided by Dorschner et al. (1995). The absorption efficiencies of amorphous olivine (MgFeSiO_4) in the form of spherical $0.5 \mu\text{m}$ sized grains are indicated with a dashed line, while the spherical grains with sizes $\leq 0.1 \mu\text{m}$ are indicated with the dash-dotted line. The dotted line represents nonspherical amorphous olivine grains. The solid line gives the absorption efficiencies of spherical $0.1 \mu\text{m}$ sized pyroxene ($\text{MgFeSi}_2\text{O}_6$), and the triple-dot-dashed line indicates the values for nonspherical pyroxene grains.

the form of spherical grains small in size compared to the wavelength (the Rayleigh limit), provide a good fit to the $10 \mu\text{m}$ feature (Vriend 1999). It is even possible to exclude the presence of a high fraction of larger grains, as well as more than 1% of the mass in the form of forsterite, based on this spectrum (Bouwman et al. 2001). We find, however, that the fit using just amorphous olivine can be further improved by adding amorphous pyroxene (also in small spherical grains). This is consistent with the suggestion that part of the silicates in the ISM are converted from olivines into pyroxenes to explain the pyroxene presence in protostars (Demyk et al. 2000).

Our result that spherical grains smaller than $\sim 0.1 \mu\text{m}$ are responsible for the $10 \mu\text{m}$ absorption feature is more or less consistent with the ISM grain size distribution determined by Mathis et al. (1977), which has an upper limit of $0.25 \mu\text{m}$. Based on a *ROSAT* study of the X-ray scattering halo of Nova Cygni 1992, Witt et al. (2001) found that they needed to extend the Mathis et al. (1977) grain size distribution to sizes much larger than $0.25 \mu\text{m}$ in order to explain the observed scattering halo. In contrast, the same observations led Draine & Tan (2003) to conclude they did not need such large grains; grains with sizes larger than $0.4 \mu\text{m}$ accounted for only a small amount of the observed scattering. Still a significant contribution to the scattering is caused by the 0.1 – $0.4 \mu\text{m}$ sized grains, while these grains do not really contribute to the $10 \mu\text{m}$ silicate absorption profile discussed in this study. Of course, the determination of grain sizes through X-ray scattering is weighted toward larger grain sizes, since those grains dominate the forward scattering cross section, while the infrared absorption profile is determined by the volume weighted average of the silicate grain size distribution, putting less weight on this discrepancy between the IR and X-ray results.

The best fit (lowest χ^2 value) of the $10 \mu\text{m}$ feature using small spherical olivine and pyroxene grains is given in Figure 4a. We find that olivine contributes 84.9% by mass and pyroxene 15.1%, for a fit of the $10 \mu\text{m}$ feature between 8.3 and $12.3 \mu\text{m}$. The remaining residues are at most on the order of $\tau \approx 0.1$, which is about 3% of the optical depth in the $10 \mu\text{m}$ feature itself. These results were achieved using only the amorphous silicates with number ratio $\text{Mg}/\text{Fe} = 1$. Dorschner et al. (1995) have measured the optical properties of amorphous pyroxenes $\text{Mg}_x\text{Fe}_{(1-x)}\text{SiO}_3$, with $x = 0.4, 0.5, 0.6, 0.7, 0.8$,

0.95, and 1.0 and olivines $\text{Mg}_{2-x}\text{Fe}_{2(1-x)}\text{SiO}_4$ with $x = 0.4$ and 0.5 . The synthesis of silicates with values of x outside the listed range (i.e., $x \leq 0.3$ for the pyroxenes and $x \geq 0.6$ for the olivines) resulted in the formation of crystalline rather than amorphous silicates (C. Jäger 2001, private communication). The spectral differences within the pyroxene and olivine family are smaller than the differences between those families. We have determined the χ^2 and χ^2_ν values for several amorphous silicate mixtures and found that only a few combinations led to an improvement according to the F -test. The F -values are only modest (on the order of 200 at most) compared to the improvements achieved when the crystalline silicates are added (see Table 3) and indicate that the pyroxenes are probably slightly Mg-rich, with a composition between $\text{Mg}_{0.5}\text{Fe}_{0.5}\text{SiO}_3$ and $\text{Mg}_{0.6}\text{Fe}_{0.4}\text{SiO}_3$. Although the sampling of the olivines is limited, the fit to the $10\ \mu\text{m}$ feature improves marginally ($F_\nu \approx 100$) when $\text{Mg}_{0.8}\text{Fe}_{1.2}\text{SiO}_4$ is added to the mixture of dust components, indicating a slightly Fe-rich composition. Since the improvements are very small, and the composition is very close to a Mg/Fe ratio of unity, we consider only the amorphous silicates with $x = 0.5$ in the remainder of this analysis.

In the case of the amorphous silicates, we have solved equation (1) using extinction efficiencies Q rather than mass absorption coefficients κ . We find that for the given dust composition and wavelength interval over which the fit is performed the derived mass fractions of 84.9% and 15.1% for olivine and pyroxene, respectively, are accurate within 0.1% with a confidence of more than 99.99%. In other words, the ratio olivine:pyroxene = 5.6:1. However, when crystalline silicates are added (see § 3.3), we find that the ratio between amorphous olivines and pyroxenes may vary, from 5.6:1 to 4.8:1.

On the basis of this fit, we can not only determine the relative masses of olivine and pyroxene, but also the column densities of the amorphous silicates toward the GC, and hence the silicate density in the diffuse ISM averaged over this line of sight.

3.2.1. The Abundance of Si

The silicate mass column density N_{sil} in the diffuse ISM is given by

$$N_{\text{sil}} = \left(\frac{4a\rho_s}{3} \right) \left(\frac{\tau_{9.7}}{Q_{9.7}} \right) \quad (4)$$

with ρ_s being the specific density of the mineral the grains are made of. The continuum-subtracted optical depth is given by $\tau_{9.7}$, while $Q_{9.7}$ is the continuum-subtracted extinction efficiency. The parameter a gives the radius of the grain, and the distance to Sgr A* is represented by L . The densities ρ_s are $3.71\ \text{g cm}^{-3}$ and $3.2\ \text{g cm}^{-3}$ for olivine and pyroxene, respectively (Dorschner et al. 1995). We find that the mass column density of olivines in the diffuse ISM $N_{\text{oliv}} = 1.3 \times 10^{-3}\ \text{g cm}^{-2}$. For the pyroxenes we find $N_{\text{pyr}} = 2.2 \times 10^{-4}\ \text{g cm}^{-2}$. These two interstellar silicate components add up to a total column density of $N_{\text{sil}} = 1.5 \times 10^{-3}\ \text{g cm}^{-2}$.

Under the assumption of solid grains, we find that the column density of Si atoms contained in silicates in the diffuse line of sight toward the GC is $N(\text{Si in silicates}) = 5.6 \times 10^{18}\ \text{cm}^{-2}$. A recent estimates for the column densities of neutral hydrogen based on X-ray scattering yields $N(\text{H}) = 1 \times 10^{23}\ \text{cm}^{-2}$ (Baganoff et al. 2003). Adopting this value, the abundance of Si in silicates is $[N(\text{Si in silicates})/N(\text{H})] = -4.25$, which is

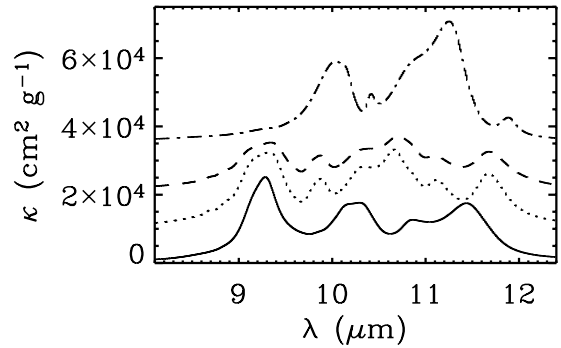


FIG. 6.—Mass absorption coefficients κ of the considered crystalline silicates. The values for diopside (solid line; Koike et al. 2000), clino-enstatite (dotted line, offset by $1 \times 10^4\ \text{cm}^2\ \text{g}^{-1}$), ortho-enstatite (dashed line, offset by $2 \times 10^4\ \text{cm}^2\ \text{g}^{-1}$) and forsterite (dash-dotted line, offset by $3.5 \times 10^4\ \text{cm}^2\ \text{g}^{-1}$; Koike et al. 1999) are shown. These mass absorption coefficients are used to determine the crystalline fraction in the studied interstellar line of sight (see Fig. 4).

somewhat higher than the *total* Si abundance of ~ -4.4 found in the solar neighborhood (Sofia et al. 1994). Porosity of the silicate grains is suggested as an explanation, because porous grains appear to have stronger $9.7\ \mu\text{m}$ resonances relative to A_V (Mathis 1998; Iati et al. 2001). This is supported by observations of the ratio $A_V/\tau_{9.7} \approx 19$ averaged over several sight lines (e.g., Roche & Aitken 1984; Mathis 1998), while this ratio seems to be ~ 10 toward the GC. On the other hand, it seems unlikely that grain properties in the GC line of sight are different from other sight lines, and a more likely explanation may be found in the enhanced metallicity in the inner region of the Galaxy, which could easily explain the slight overabundance observed toward Sgr A*. This is supported by the observations summarized in Figure 5.8 of Whittet (2003).

3.3. The Crystalline Fraction in the Diffuse ISM

We determined the degree of crystallinity by adding the mass absorption coefficients of some crystalline silicates to the sum in equation (1). We have limited our search to the components already identified to be present in astrophysical environments. These are forsterite, clino- and ortho-enstatite, and diopside. For consistency, we adopted the measurements obtained in one experimental set-up. Since diopside is only measured in one laboratory (Koike et al. 2000), we thus used the mass absorption coefficient (κ) measurements of clino- and ortho-enstatite and forsterite from the same laboratory (Koike et al. 1999). The measurements were obtained from minerals crushed in a mortar, leading to nonspherical grain shapes. The grains larger than $0.5\ \mu\text{m}$ in size were removed, and the remaining grains were incorporated in a KBr pellet. When using the mass absorption coefficients κ from these experiments, we assume that the grain shape and size distribution of the sample resembles that of the crystalline silicates in the ISM.

The small residues remaining when the fit with only amorphous silicates was performed suggest that there is not much room for crystalline silicates left. The mass fraction of crystalline silicates is probably considerably less than 3% (the level of the residues compared to the total optical depth) because the resonances produced by crystalline silicates in the $10\ \mu\text{m}$ region are not only much narrower (see Fig. 6) but also intrinsically much stronger than the resonances due to amorphous silicates.

The κ values of all four species of crystalline silicates are included in equation (1). We have minimized χ^2 and find that

TABLE 2
IMPROVEMENTS OF THE SPECTRAL FIT ACHIEVED BY ADDING NEW DUST COMPONENTS

Initial Dust Component (1)	Added Dust Component (2)	$\Delta\chi^2$ (3)	χ^2_ν (4)	F_χ (5)	Olivine (%) (6)	Pyroxine (%) (7)	Forsterite (%) (8)	Diopside (%) (9)	Clino-enstatite (%) (10)	Ortho-enstatite (%) (11)
Amorphous.....	69.9	...	84.9	15.1
Amorphous.....	Forsterite	40007	44.5	900	82.7	17.1	0.2
Amorphous.....	Diopside	11024	62.9	175	84.3	15.4	...	0.3
Amorphous.....	Clino-enst.	<0	...	<0
Amorphous.....	Ortho-enst.	552	69.6	7.9	84.7	15.2	0.07
Amorphous +forsterite.....	Diopside	139	44.4	3.1	82.7	17.1	0.2	0.03

NOTES.—The improvement is considered significant when F_χ is large (see text). Col. (1) gives the initial dust components, while the newly added dust component is given in col. (2). The change in χ^2 is given in col. (3), and the reduced χ^2_ν corresponding to the best fit with the new dust component added is presented in the col. (4). Col. (5) gives the value for F_χ . Cols. (6)–(11) give the relative abundance of each dust component corresponding to the new best fit. Only adding forsterite or diopside significantly improves the fit. The first line of data gives the best values for a completely amorphous dust composition.

the best fit is given by a crystalline over amorphous fraction of 0.2% by mass. The composition of crystalline silicates found in this best fit is dominated mostly by forsterite, while $\sim 1/6$ of the crystalline silicates are in the form of either diopside or enstatite. It is hard to distinguish between the contributions of the various crystalline pyroxenes, as their strongest resonance at $\sim 9.2 \mu\text{m}$ largely overlaps. On the other hand, the olivines are easily distinguished from the pyroxenes, because of the presence of a strong resonance at $\sim 11.2 \mu\text{m}$.

In order to determine the amount of each individual crystalline dust component that could be present, we have added them separately to the amorphous mixture and determined the best χ^2 fit. The F -test was performed to determine the significance of adding these different dust components. The results are shown in Table 2. We find that the most significant improvement is achieved when forsterite is added to a completely amorphous mixture, resulting in an F -value of 900. A smaller improvement, but still significant, is achieved by adding diopside to a completely amorphous composition. Adding ortho-enstatite does not lead to a very significant improvement, which can be concluded from the small F -value (see § 3.1). Adding clino-enstatite does not improve the fit at all. When diopside is added to a mixture of amorphous silicates and forsterite also only a minor improvement is achieved.

To study the significance of the result that 0.2% of the silicates are crystalline, we have constructed a variety of dust compositions, ranging from 0.1% to 3% in degree of crystallinity x . We used a mass ratio of 5.6:1 for amorphous olivine : pyroxene, and a ratio of 6:1 for forsterite : (enstatite+diopside). We assumed that diopside and enstatite were present in equal amounts. For each of these crystallinities, the best fits by minimizing the χ^2 and χ^2_ν value are obtained and compared with the fit for 0% crystallinity by performing the F -test. The results are given in Table 3. For $x \leq 0.4\%$, the χ^2_ν fit has improved compared to the purely amorphous dust composition. Since all the $F_\chi \gg 1$, the improvement of the fit is significant. For $x > 0.4\%$, the fit deteriorates quickly with increasing x , and the resulting F -values are negative. Examination of the residuals allows us to firmly determine that the degree of crystallinity of silicates in the diffuse ISM is $\leq 0.4\%$. In Figure 4 some sample residuals are shown. For $x \geq 0.5\%$ for example, the overabundance of crystalline silicates clearly appears in the residuals and in the model spectrum. Hence, we derive that the degree of crystallinity in the diffuse interstellar medium is $0.2\% \pm 0.2\%$.

Although $x = 0.2\%$ gives the best fit to the optical depth in the $10 \mu\text{m}$ silicate feature, we would like to point out that this number may be an upper limit as well. It is mostly determined by the $11.2 \mu\text{m}$ forsterite feature. Other possible interstellar dust components such as PAHs, carbonates, water ice, and SiC have strong resonances near this wavelength too, which may account for part of the optical depth at that particular wavelength, thus decreasing the contribution and mass fraction of crystalline silicates.

From this analysis it becomes clear that forsterite may be present in the diffuse ISM, at a mass fraction of at most 0.2%. The other crystalline components only contribute in minor amounts.

3.4. Other Dust Components

Besides crystalline silicates, several other dust components have resonances overlapping with the wavelength range covered by the amorphous silicate absorption feature. Of high astrophysical interest is silicon carbide (SiC), a dust component commonly produced by carbon-rich asymptotic giant branch (AGB) stars. In a similar fashion as described here, the mass of SiC with respect to silicates can be determined and

TABLE 3
OVERVIEW OF THE FIT RESULTS FOR VARIOUS DEGREES OF CRYSTALLINITY

x (1)	χ^2_ν (2)	F_χ (3)
0.0.....	70	...
0.1.....	56	396
0.2.....	51	549
0.3.....	58	338
0.4.....	72	<0
0.5.....	96	<0
0.7.....	168	<0
1.0.....	331	<0
1.5.....	723	<0
2.0.....	1231	<0
3.0.....	2470	<0

NOTES.—Col. (1) represents the mass fraction x of the silicates that is crystalline, col. (2) gives the minimized value of χ^2_ν determining the best fit. In case the χ^2_ν has decreased compared to the value corresponding to $x = 0$, the goodness of the fit was evaluated using the F -test (col. [3]). For $F_\chi \gg 1$ adding the crystalline silicates as an extra parameter really improved the fit.

TABLE 4
CONTRIBUTION OF DUST-PRODUCING STARS TO THE CRYSTALLINE SILICATE REPLENISHMENT OF THE ISM

Type of Star (1)	N (kpc ⁻²) (2)	\dot{M}_{dust} (M_{\odot} yr ⁻¹) (3)	x (%) (4)	\dot{M}_{inj} (M_{\odot} yr ⁻¹ kpc ⁻²) (5)	$(x \dot{M}_{\text{inj}})/\dot{M}_{\text{ISM}}$ (%) (6)
Miras	11.4 ^{a,b}	10 ⁻⁹	<40 ^c	1.14 × 10 ⁻⁸	<0.2
OH/IR stars	1.1 ^{a,b}	10 ⁻⁶	10 ^c	1.1 × 10 ⁻⁶	4–5
M supergiants.....	1–2 ^d	10 ⁻⁶	15–20 ^e	(1–2) × 10 ⁻⁶	7–13
Supernovae.....	n/a	n/a	?	~4 × 10 ^{-7f}	?

NOTES.—Col. (1) gives the surface number density of each type of silicate dust producing star in the solar vicinity. Col. (2) gives the dust mass loss rate, assuming a dust/gas ratio of 1/100. Col. (3) gives the mass fraction of crystalline silicates in the stellar outflow. Col. (4) gives the mass injection rate in the ISM, which is in fact the product of the numbers in cols. (1) and (2). Col. (5), then, gives the crystalline silicate injection into the ISM, relative to the total silicate injection rate. The total degree of crystallinity of the silicates injected into the ISM is the sum of the numbers in col. (5).

^a Jura & Kleinmann (1989).

^b Habing (1996).

^c Kemper et al. (2001).

^d Jura & Kleinmann (1990).

^e Molster et al. (1999).

^f Whittet (2003).

compared to the dust mass ratio produced by carbon stars versus oxygen stars. Indeed, Whittet et al. (1990) were able to determine that the abundance of Si atoms in interstellar SiC was less than 5% of the abundance of Si in interstellar silicates, which translates into a mass fraction taken by SiC of less than 1.7% of the total Si-containing dust. This result is based on low-resolution 7.5–13.5 μm spectroscopy of GC sources (Roche & Aitken 1985). Whittet et al. (1990) conclude that SiC is probably destroyed upon ejection into the ISM on a timescale of $\sim 5 \times 10^7$ yr.

We have used the optical properties presented by Laor & Draine (1993) to calculate how many spherical SiC grains with radius 0.1 μm could be present in the line of sight toward the GC. A strong resonance at ~ 10.6 μm may be used to determine the abundance of SiC in the diffuse ISM. We find that adding the opacity of SiC to a mixture of amorphous silicates or to a mixture of amorphous and crystalline silicates only deteriorates the fit, leading to negative F_{χ} -values. Our conclusion is that 0.1 μm sized spherical SiC grains make up less than 0.1% of the interstellar Si-bearing dust mass. This is a factor of 17 better than the previous determination based on ground-based 10 μm spectra (Whittet et al. 1990). Analysis of this result requires the use of reliable optical properties of SiC, which are currently unavailable (Speck et al. 1999). In a future study we will re-address this issue (F. Kemper & A. Speck 2004, in preparation).

4. SILICATE PROCESSING IN THE DIFFUSE ISM

4.1. Injection of Circumstellar Silicates

It is generally believed that AGB stars and red supergiants dominate the production of oxygen-rich dust in the Galaxy (see, e.g., Whittet 2003 and references therein). Most oxygen-rich dust produced by these stars is in the form of silicates. The density of M supergiants is found to be 1–2 kpc⁻² (Jura & Kleinmann 1990) projected on the Galactic plane, while the density of AGB stars is ~ 25 kpc⁻² (Jura & Kleinmann 1989). Almost all supergiants and about half of the AGB stars produce silicate dust. Since OH/IR stars occur 10 times less frequently than Miras (Habing 1996), we can infer that the density of Miras is ~ 11.4 kpc⁻², while the density of OH/IR stars is ~ 1.1 kpc⁻². Adopting a typical mass-loss rate of $10^{-7} M_{\odot}$ yr⁻¹ for the Miras and $10^{-4} M_{\odot}$ yr⁻¹ for the M supergiants and

OH/IR stars (see, e.g., Habing 1996 and references therein) and assuming that the dust-to-gas ratio is 0.01, we are able to determine the dust injection rate (Table 4). We assume that all oxygen-rich dust produced by these stars is in the form of silicates. The crystalline fraction of AGB stars is relatively well known. It is estimated that about 10% of the silicates around OH/IR stars are crystalline, while for the Miras only an upper limit of 40% of the crystallinity can be derived (Kemper et al. 2001). The degree of crystallinity in the spectra of M supergiants is less well known, in part because most of those dust shells are optically thin and may be able to hide a large amount of crystalline silicates in a similar way as described in Kemper et al. (2001). We use the supergiant AFGL 4106 as an example and adopt the derived crystallinity of 15%–20% (Molster et al. 1999) as a typical value. Hence, the crystallinity of the silicates in the combined stellar ejecta will be 11%–18%, where 4%–5% originates from OH/IR stars and 7%–13% from M supergiants. The contribution from Miras is negligible (Table 4). One has to realize that most of these estimates are based on a few objects, and the degree of crystallinity of stellar ejecta is inherently an uncertain number.

The degree of crystallinity of silicates in the ejecta of stars (11%–18%) contributing to the interstellar dust budget is significantly different from the crystallinity observed in interstellar silicates ($0.2\% \pm 0.2\%$). We explore two possible explanations for this discrepancy. We mainly focus on the possibility that an amorphization process occurs on timescales significantly shorter than the destruction timescales, in order to decrease the degree of crystallinity, specifically amorphization by cosmic ray hits or particle bombardment (§ 4.2). In addition, we consider the possibility that the crystalline fraction in stellar ejecta is diluted by a yet neglected source of amorphous silicates, greatly decreasing the average crystallinity of newly synthesized dust (§ 4.3). We discuss the dust production by supernovae, recently suggested to be a significant source of Galactic dust (Dunne et al. 2003).

4.2. Amorphization in the Diffuse ISM

In previous studies (e.g., Jones et al. 1994) the grain destruction rates and dust life time in the ISM have been estimated. However, to date, the rates and timescales involved

with crystallization and amorphization in interstellar conditions have not yet been addressed. In this work, we derive an expression for the grain amorphization rate, and we compare this to laboratory experiments on the amorphization of grains in astrophysical conditions.

The total mass of crystalline and amorphous silicates in the ISM can be written in the form of coupled differential equations:

$$\begin{cases} \frac{dM_X}{dt} = x_* \dot{M}_* - k_1 M_X + k_2 M_A - k_3 M_X, \\ \frac{dM_A}{dt} = (1 - x_*) \dot{M}_* + k_1 M_X - k_2 M_A - k_3 M_A, \end{cases} \quad (5)$$

where M_X and M_A represent the crystalline and amorphous silicate mass in the ISM, respectively; \dot{M}_* is the injection rate of stellar silicates assumed to be constant over time, with x_* the mass fraction of stellar silicates that are crystalline, which is also constant. The amorphization rate is given by k_1 , the crystallization rate by k_2 , and the destruction rate by k_3 . Under interstellar conditions, k_2 will be very small, and therefore we assume it to be 0. We assume that at the current time equilibrium is reached, which implies the stationary solution, i.e.,

$$\begin{cases} \frac{dM_X}{dt} = 0, \\ \frac{dM_A}{dt} = 0. \end{cases} \quad (6)$$

By combining equations (5) and (6), it is possible to determine k_1 and k_3 , assuming $k_2 = 0$. We find that

$$k_1 = k_3 \frac{x_* - x_{\text{ISM}}}{x_{\text{ISM}}} \quad (7)$$

and

$$k_3 = \frac{\dot{M}_*}{M_X + M_A}, \quad (8)$$

where x_{ISM} is the mass fraction of silicates in the ISM that has a crystalline lattice structure, given by $x_{\text{ISM}} = M_X / (M_A + M_X)$.

For silicate grains the destruction rate k_3 is $\sim 2 \times 10^{-9} \text{ yr}^{-1}$, corresponding to a dust lifetime of $4 \times 10^8 \text{ yr}$ (Jones et al. 1994, 1996), although Tielens (1998) derives a significantly shorter lifetime of $6 \times 10^7 \text{ yr}$, using observed depletions. Adopting the longest timescale of $4 \times 10^8 \text{ yr}$ as a conservative choice, the measured crystallinities $x_{\text{ISM}} = 0.002$ and $x_* = 0.15$ require an amorphization rate k_1 of $1.5 \times 10^{-7} \text{ yr}^{-1}$ to reach a final crystallinity of 0.2%. This corresponds to an amorphization timescale of $\sim 5 \text{ Myr}$. Because the upper limit to the crystallinity of the silicates in the ISM is 0.4%, the amorphization rate should be faster than $7.3 \times 10^{-8} \text{ yr}^{-1}$, corresponding to a timescale of $\sim 9 \text{ Myr}$ or shorter. Better determinations of the degree of crystallinity of the silicates in stellar ejecta may yield a change in the amorphization timescale. The timescales derived here should therefore be treated only as estimates.

The most likely process to cause amorphization on timescales of $\sim 5 \text{ Myr}$ are ion bombardments of incident particles on crystalline grains. Studies of dust grains collected by the Apollo astronauts on the surface of the moon suggest that amorphization by ion bombardments occurs. These studies have revealed that most grains are surrounded by a 60–200 nm thick amorphous rims. It is suggested that these rims are caused by solar wind radiation damage, during the relatively short

period (5000–10,000 yr) that each particular grain was exposed to it before the grain was covered by other extralunar grains deposited on the moon's surface (Borg et al. 1980). Although other mechanisms for the amorphization have been suggested, such as the deposition of vapor phase materials after the impact of a meteorite on the surface of the moon (Keller & McKay 1993), it is thought that at least part of the amorphous material found on the moon is the result of damage by particles from the solar wind (Keller & McKay 1997).

To date, several laboratory studies have investigated the effect of ion bombardments on crystalline grains (e.g., Day 1977; Bradley 1994; Wang et al. 1998; Demyk et al. 2001; Carrez et al. 2002; Jäger et al. 2003b; Brucato et al. 2004), measuring the required dose for amorphization as a function of energy and element used. In general, the dose D_n (eV cm^{-3}) can be written as

$$D_n = \Phi S_n, \quad (9)$$

where Φ (cm^{-2}) is the particle fluence and S_n (eV cm^{-1}) the stopping power. From the compilation of experimental data presented by Brucato et al. (2004), it becomes clear that for 30–60 keV ions 80% disorder is achieved for doses over $20 \times 10^{23} \text{ eV cm}^{-3}$. In this regime, the experiments are dominated by nuclear stopping power. The stopping powers S_n for the ions considered are $S_n(30 \text{ keV H}^+) \approx 0.08 \text{ eV \AA}^{-1}$, $S_n(30 \text{ keV He}^+) \approx 0.8 \text{ eV \AA}^{-1}$, and $S_n(60 \text{ keV Ar}^{2+}) \approx 90 \text{ eV \AA}^{-1}$ (Brucato et al. 2004). The Ar^{2+} abundance is not known for these low-energy cosmic rays, but using intermediate and high-energy measurements, as well as cosmic abundances of the elements, we estimate that the abundance with respect to He is $[\text{Ar}/\text{He}] \approx -4$ (see, e.g., Wefel 1988). Although Ar^{2+} is not very abundant in cosmic rays, it actually deposits a large amount of energy over a short distance. The particle flux necessary to achieve the required dose for amorphization follows from equation (9), and we find that $\Phi = 2.2 \times 10^{14} \text{ cm}^{-2}$, to be collected over less than $\sim 9 \text{ Myr}$. Extrapolating using equation (3) from Brucato et al. (2004), we obtain an estimate that the intensity of particles with energies of 60 keV equals 1 particle $\text{cm}^{-2} \text{ s}^{-1} \text{ sr}^{-1}$, although this formula has not been verified for this energy range. Integrating over an entire sphere and over the maximum amorphization timescale of 9 Myr, we find that a grain has seen 3.5×10^{15} particles cm^{-2} , containing a dose of less than $3.5 \times 10^{11} \text{ Ar}^{2+}$ ions cm^{-2} . This is not sufficient to amorphitize a crystalline grain by means of Ar^{2+} bombardment. It has been suggested that the more abundant Fe^{2+} ions ($[\text{Fe}/\text{He}] \approx -3$; see Wefel 1988) might be able to explain the amorphization. The stopping power of a 60 keV Fe^{2+} ion is 75 eV \AA^{-1} (E. Bringa 2003, private communication); however, the required dose of Fe^{2+} for amorphization remains yet to be experimentally determined, although calculations of the amorphization process are well on their way (Bringa & Johnson 2002; Bringa & Johnson 2004). Processing by the abundant C, N, O ions may contribute to the amorphization as well. Finally, as stated before, the ion flux in the keV regime is not known and remains subject to further study. The amorphization timescale may in fact provide a constraint on the ion flux in the keV regime.

4.3. Dilution of Stellar Ejecta

A significant source of silicate dust may be the product of supernovae. Recently, it has been suggested that Type II supernovae (Dunne et al. 2003) and Type Ib supernovae (Morgan et al. 2003) can produce on the order of a solar mass of dust

per supernova, which is much higher than what is generally accepted (Whittet 2003; see also Table 4). These new results are based on SCUBA/JCMT photometry at 450 and 850 μm of Cas A and Kepler's supernova remnant, respectively. The submillimeter photometry requires a cold dust component (in addition to the warm dust component traced by *IRAS* photometry) to explain the spectral energy distribution. Although the authors argue that this dust is produced by the supernovae, it may also be swept-up interstellar dust. Depending on the choice of far-infrared/submillimeter dust emissivities, it is estimated that Cas A is surrounded by $2\text{--}4 M_{\odot}$ of cold dust, while Kepler's supernova remnant contains $\sim 1 M_{\odot}$ in the form of cold dust. It is debatable whether two data points provide sufficient information to constrain the complex physical environment in a supernova remnant, where the number of free parameters is only constrained by one's imagination, and describe properties such as geometry, density distribution, clumpiness, grain properties, dust composition, and the interaction with the surrounding ISM. Indeed, Dwek (2004) shows that a much smaller dust mass in the form of metallic iron needles explains the same submillimeter data points. The Galactic dust production rate by supernovae is estimated to be $(7\text{--}15) \times 10^{-3} M_{\odot} \text{ yr}^{-1}$ (Dunne et al. 2003; Morgan et al. 2003), which is dominated by the cold dust. The authors have derived this rate by scaling the dust production rates for type II supernovae (Todini & Ferrara 2001) with the dust condensation efficiency determined for Cas A, assuming it had a $30 M_{\odot}$ progenitor, and applying a supernova rate, which arises from standard values of the initial mass function and star formation rate (L. Dunne 2003, private communication). When this supernova dust production rate is compared with the production rate from other stars ($\sim 5 \times 10^{-3} M_{\odot} \text{ yr}^{-1}$; Whittet 2003), one can conclude that 60%–75% of the Galactic dust originates from supernovae.

Unfortunately, the two SCUBA data points used for this determination do not yield any information on the composition of this cold dust component. The presence of a 22 μm feature in the warm dust component of Cas A is reported (Arendt et al. 1999), which is attributed to a Mg-protosilicate. Mg-protosilicate is a MgO/SiO₂ gel formed in a solution of Na-silicate and MgCl₂ (Day 1974), which can be seen as a Mg-rich amorphous silicate.

In order to estimate an upper limit on the dilution, we assume that all dust produced by supernovae comes out in the form of amorphous silicates. Thus, if we adopt that 60%–75% of the Galactic dust originates from supernova, and that the remaining 25%–40% produced by evolved stars has a degree of crystallinity of 11%–18%, one easily sees that in the case of the most efficient dilution, the combined stellar ejecta still have a degree of crystallinity of 3%–7%, which is still more than an order of magnitude larger than the observed crystallinity of $(0.2\% \pm 0.2\%)$ observed for silicates in the diffuse ISM. Clearly, dilution by supernova dust does not fully explain the low degree of crystallinity observed in the diffuse ISM, although it may contribute to some extent.

We will not consider dilution by silicates formed in the diffuse ISM. In the low-density environment of the diffuse ISM, the formation of amorphous silicates from gas phase molecules is unlikely, although the high depletion of Si and high grain destruction rate suggest that grain formation occurs (Jones et al. 1994; Draine 2003). The observed difference in depletion between cloud- and intercloud-regions in the ISM (see, e.g., Sofia et al. 1994) show that dust destruction and formation commonly occurs in the ISM (Tielens 1998).

5. COMPARISON WITH PRESOLAR GRAINS, YOUNG STARS, AND THE DENSE INTERSTELLAR MEDIUM

Crystalline silicates are reported to be present in the dense interstellar environment, based on the identification of features in the *ISO* spectra. While the presence of crystalline silicates in circumstellar environments is well established, their presence in the dense ISM remains subject to discussion. Dense ISM crystalline silicates were first reported to be present in Orion (Cesarsky et al. 2000), but the features ascribed to crystalline silicates in this work may very well be explained by a combination of a PAH emission plateau, memory effects in the data, and incorrect band merging (F. Kemper 2004, in preparation). Onaka & Okada (2003) report on the detection of diopside in the Carina H II region, based on the identification of the 60 μm feature by diopside. In other environments, other identifications of this feature have been suggested, including water ice around evolved stars (Barlow 1998) and dolomite in planetary nebulae (Kemper et al. 2002), and recent measurements of melilite also look promising as an identification of the 60 μm feature (Chihara et al. 2004). Even though there are some indications that crystalline silicates are present in dense clouds associated with young stellar objects, at most 1%–2% of the silicates seen in the lines of sight toward protostars can have a crystalline lattice structure (Demyk et al. 1999).

Crystalline silicates are often found in the direct circumstellar environments of pre-main-sequence stars and young main-sequence stars. They are detected in debris disk object β Pic (Knacke et al. 1993), in some T Tauri stars (Honda et al. 2003), and are quite common in the more massive Herbig Ae/Be stars (e.g., Bouwman et al. 2001; Meeus et al. 2001). To date, no crystalline silicates have been found in the younger, deeply embedded class 0 objects (Demyk et al. 1999).

The lack of crystalline silicates in the diffuse ISM suggests that crystalline silicates found in environments associated with star formation and dense clouds are formed or annealed locally. There might have been an exchange of crystalline silicates between dense clouds, cloud cores, and circumstellar disks, but any excursion into the diffuse ISM would make a crystalline silicate amorphous on a very short timescale.

In the solar system, cometary dust particles are generally believed to be the most pristine dust particles, which survived the formation of the solar system without being processed. Infrared spectroscopy of comets and laboratory analysis of cometary dust particles has revealed that comets contain a considerable fraction of crystalline silicates, usually around 30%. The remainder of the silicates are found to be amorphous (Wooden 2002 and references therein). Recent model calculations, however, suggest that the amount of crystalline silicates in comet Hale-Bopp may be significantly lower than previously assumed (M. Min 2004, in preparation). The crystallization of these cometary silicates must have occurred after the grain left the diffuse ISM, either in the dense molecular cloud during the star formation process or in the solar nebula, and thus cometary grains do not represent unaltered interstellar dust. Another way to study cometary dust is by collecting interplanetary dust particles (IDPs) of cometary origin in the stratosphere of the Earth. Both the remote observations of comets and the study of IDPs suggest that the crystalline fraction in comets is much larger than in the ISM. That suggests perhaps whole-scale recrystallization and mixing in the solar nebula has occurred, in which grains are evaporated and recondensed in the crystalline form.

Messenger et al. (2003) have studied a sample of nine anhydrous IDPs collected by NASA over a number of years and were able to identify 1031 individual silicate subgrains. Six of these grains have nonsolar oxygen isotopic compositions, indicating a presolar origin of these grains. The isotopic ratios point to formation by red supergiants or AGB stars. It is important to realize that grains with an isotopic composition that resembles the solar composition may have condensed in the presolar nebula but could also originate from the prestellar nebulae of young stellar objects in the vicinity of the solar nebula. The six grains of nonsolar isotopic composition therefore only represent a lower limit to the number of presolar or interstellar grains in the sample. For three of the grains with nonsolar isotopic ratios, the mineralogical composition has been determined; two of them are found to be GEMS grains (glasses with embedded metals and sulfides, i.e., amorphous silicates; Bradley 1994) and one turns out to be a forsterite grain. From this one might conclude that 1/6 of the interstellar grains are crystalline, which contradicts our result. The IDP study clearly suffers from small number statistics, and their result will become more significant if more data on the composition of presolar grains can be acquired.

6. CONCLUSIONS

In this work, the results of a study on the crystallinity of silicates in the diffuse ISM have been presented. It is known that crystalline silicates are common in the circumstellar environment of both pre- and post-main-sequence stars. It is generally accepted that the dust particles found in the circumstellar environment of young stars originate from evolved stars, and have arrived in their current location after a long (several Gyr) residence time in the ISM. The puzzling lack of evidence of crystalline silicates in the ISM prompted us to set a firm upper limit on the crystallinity.

Studying the 10 μm silicate feature in absorption toward Sgr A*, we are able to determine that at most 0.4% of the silicates in the ISM have a crystalline structure. The data are best fitted with a degree of crystallinity of 0.2%. In addition, we have determined the composition of the amorphous silicate component in the diffuse ISM. We found that 84.9% of the amorphous grains are olivine ($\text{Mg}_{2x}\text{Fe}_{2(1-x)}\text{SiO}_4$) and 15.1% are pyroxene ($\text{Mg}_x\text{Fe}_{(1-x)}\text{SiO}_3$). The amorphous grains were found to be spherical and smaller than $\sim 0.1 \mu\text{m}$ in radius.

Detailed analysis of the 10 μm feature indicates that the pyroxenes are probably slightly Mg-rich (with $0.5 < x < 0.6$), and the interstellar olivines may be Fe-rich (with $0.4 < x < 0.5$).

By comparison of these results with the crystallinity of the silicates produced by mass-losing stars, and the interstellar grain destruction rate, we have determined the interstellar amorphization rate and found that crystalline silicates are effectively amorphitized in 5 Myr to achieve a final crystallinity of 0.2%, while an amorphization timescale of 9 Myr is consistent with the determined upper limit of 0.4%. These numbers are only estimates, as the crystallinity of stellar ejecta has not yet been determined very accurately.

Amorphization by low-energy ion bombardment has been explored as an explanation for the low degree of crystallinity of silicates in the ISM, but the results are not yet consistent with the observed low degree of crystallinity. In addition, dilution by other sources of amorphous silicates, such as supernovae, is not sufficient to explain the observed lack of crystalline silicates in the ISM.

We conclude that effectively all silicates in the diffuse ISM become amorphous on a very short timescale, compared to the total residence time in the diffuse ISM. Hence, the crystalline silicates found in the circumstellar environments of young stars, in the solar system, and in star formation regions have not survived the ISM unaltered but are probably crystallized locally. Both annealing and evaporation followed by condensation seem to be significant crystallization processes.

We thank Don Brownlee, Lindsay Keller, and Scott Messenger for organizing the workshop on cometary dust in astrophysics, held in Crystal Mountain, WA, in 2003 August. This work greatly benefited from the fruitful interdisciplinary interactions at this meeting. We thank Angelle Tanner for making available the 12.4 μm map of the Galactic center region. F. K. wishes to thank Mark Logan for the inspiring discussions. Support for this work was provided by NASA through the Spitzer Fellowship Program, under award 011 808-001. The data presented were analyzed with the support of the Dutch *ISO* Data Analysis Centre (DIDAC) at the Space Research Organization Netherlands (SRON) in Groningen, the Netherlands.

REFERENCES

- Arendt, R. G., Dwek, E., & Moseley, S. H. 1999, *ApJ*, 521, 234
 Baganoff, F. K., Maeda, Y., Morris, M., et al. 2003, *ApJ*, 591, 891
 Barlow, M. J. 1998, *Ap&SS*, 255, 315
 Becklin, E. E., Matthews, K., Neugebauer, G., & Willner, S. P. 1978, *ApJ*, 219, 121
 Bevington, P. R., & Robinson, D. K. 1992, *Data Reduction and Error Analysis for the Physical Sciences* (2nd ed.; New York: McGraw-Hill)
 Bohren, C. F., & Huffman, D. R. 1983, *Absorption and Scattering of Light by Small Particles* (New York: Wiley)
 Borg, J., Chaumont, J., Joutet, C., Langevin, Y., & Murette, M. 1980, in *Proc. Conf. Ancient Sun*, ed. R. O. Pepin, J. A. Eddy, & R. B. Merrill (New York: Pergamon), 431
 Bouwman, J., et al. 2001, *A&A*, 375, 950
 Bowey, J. E., & Adamson, A. J. 2002, *MNRAS*, 334, 94
 Bradley, J. P. 1994, *Science*, 265, 925
 Bringa, E. M., & Johnson, R. E. 2002, *Nucl. Instrum. Methods Phys. Res. B*, 193, 365
 ———. 2004, *ApJ*, 603, 159
 Brucato, J. R., Strazzulla, G., Baratta, G., & Colangeli, L. 2004, *A&A*, 413, 395
 Carrez, P., Demyk, K., Cordier, P., et al. 2002, *Meteoritics Planet. Sci.*, 37, 1599
 Cesarsky, D., Jones, A. P., Lequeux, J., & Verstraete, L. 2000, *A&A*, 358, 708
 Chiar, J. E., Pendleton, Y. J., Geballe, T. R., & Tielens, A. G. G. M. 1998, *ApJ*, 507, 281
 Chiar, J. E., Tielens, A. G. G. M., Whittet, D. C. B., Schutte, W. A., Boogert, A. C. A., Lutz, D., van Dishoeck, E. F., & Bernstein, M. P. 2000, *ApJ*, 537, 749
 Chihara, H., Koike, C., & Tsuchiyama, A. 2004, in *ASP Conf. Ser. 309, Astrophysics of Dust*, ed. A. N. Witt, G. C. Clayton, & B. T. Draine (San Francisco: ASP), in press
 Day, K. L. 1974, *ApJ*, 192, L15
 ———. 1977, *MNRAS*, 178, 49P
 de Graauw, T., Haser, L. N., Beintema, D. A., et al. 1996, *A&A*, 315, L49
 Demyk, K., Jones, A. P., Dartois, E., Cox, P., & d'Hendecourt, L. 1999, *A&A*, 349, 267
 Demyk, K., et al. 2001, *A&A*, 368, L38
 ———. 2000, in *ISO Beyond the Peaks: The 2nd ISO Workshop on Analytical Spectroscopy*, ed. A. Salama, M. F. Kessler, K. Leech, & B. Schulz (ESA-SP 456; Noordwijk: ESA), 183
 Dorschner, J., Begemann, B., Henning, T., Jäger, C., & Mutschke, H. 1995, *A&A*, 300, 503
 Draine, B. T. 2003, *ARA&A*, 41, 241
 Draine, B. T., & Tan, J. C. 2003, *ApJ*, 594, 347

- Dunne, L., Eales, S., Ivison, R., Morgan, H., & Edmunds, M. 2003, *Nature*, 424, 285
- Dwek, E. 2004, *ApJ*, 607, 848, 854
- Figer, D. F., McLean, I. S., & Morris, M. 1999, *ApJ*, 514, 202
- Fouks, B. I., & Schubert, J. 1995, *Proc. SPIE*, 2475, 487
- Habing, H. 1996, *Astron. Astrophys. Rev.*, 7, 97
- Honda, M., et al. 2003, *ApJ*, 585, L59
- Iati, M. A., et al. 2001, *MNRAS*, 322, 749
- Jäger, C., Dorschner, J., Mutschke, H., Posch, T., & Henning, T. 2003a, *A&A*, 408, 193
- Jäger, C., et al. 2003b, *A&A*, 401, 57
- Jones, A. P., Tielens, A. G. G. M., & Hollenbach, D. J. 1996, *ApJ*, 469, 740
- Jones, A. P., Tielens, A. G. G. M., Hollenbach, D. J., & McKee, C. F. 1994, *ApJ*, 433, 797
- Jura, M., & Kleinmann, S. G. 1989, *ApJ*, 341, 359
- . 1990, *ApJS*, 73, 769
- Keller, L. P., & McKay, D. S. 1993, *Science*, 261, 1305
- . 1997, *Geochim. Cosmochim. Acta*, 61, 2331
- Kemper, F., Waters, L. B. F. M., de Koter, A., & Tielens, A. G. G. M. 2001, *A&A*, 369, 132
- Kemper, F., et al. 2002, *Nature*, 415, 295
- Kessler, M. F., Steinz, J. A., Anderegg, M. E., et al. 1996, *A&A*, 315, L27
- Kester, D. J. M. 2003, in *The Calibration Legacy of the ISO Mission*, ed. L. Metcalfe, A. Salama, S. B. Peschke, & M. F. Kessler (ESA SP-481; Noordwijk: ESA), 243
- Knacke, R. F., Fajardo-Acosta, S. B., Telesco, C. M., et al. 1993, *ApJ*, 418, 440
- Koike, C., Tsuchiyama, A., & Suto, H. 1999, in *Proc. 32nd ISAS Lunar and Planetary Symp.*, ed. H. Mitzutani & M. Kato (Kanagawa: ISAS), 175
- Koike, C., et al. 2000, *A&A*, 363, 1115
- Laor, A., & Draine, B. T. 1993, *ApJ*, 402, 441
- Leech, K., et al., ed. 2003, *The ISO Handbook*, Vol. V: SWS—The Short Wavelength Spectrometer, ver. 2.0.1 (Noordwijk: ESA)
- Li, A., & Draine, B. T. 2001, *ApJ*, 550, L213
- Lutz, D., et al. 1996, *A&A*, 315, L269
- Mathis, J. S. 1998, *ApJ*, 497, 824
- Mathis, J. S., Ruml, W., & Nordsieck, K. H. 1977, *ApJ*, 217, 425
- Meeus, G., et al. 2001, *A&A*, 365, 476
- Messenger, S., Keller, L. P., Stadermann, F. J., Walker, R. M., & Zinner, E. 2003, *Science*, 300, 105
- Molster, F. J., Waters, L. B. F. M., Tielens, A. G. G. M., & Barlow, M. J. 2002, *A&A*, 382, 184
- Molster, F. J., et al. 1999, *A&A*, 350, 163
- Moneti, A., Stolovy, S., Blommaert, J. A. D. L., Figer, D. F., & Najaro, F. 2001, *A&A*, 366, 106
- Morgan, H. L., Dunne, L., Eales, S. A., Ivison, R. J., & Edmunds, M. G. 2003, *ApJ*, 597, L33
- Onaka, T., & Okada, Y. 2003, *ApJ*, 585, 872
- Pendleton, Y. J., Sandford, S. A., Allamandola, L. J., Tielens, A. G. G. M., & Sellgren, K. 1994, *ApJ*, 437, 683
- Press, W. H., Teukolsky, S. A., Vetterling, W. T., & Flannery, B. P. 1992, *Numerical Recipes in Fortran 77* (2nd ed.; Cambridge: Cambridge Univ. Press)
- Rieke, G. H., Rieke, M. J., & Paul, A. E. 1989, *ApJ*, 336, 752
- Roche, P. F., & Aitken, D. K. 1984, *MNRAS*, 208, 481
- . 1985, *MNRAS*, 215, 425
- Sofia, U. J., Cardelli, J. A., & Savage, B. D. 1994, *ApJ*, 430, 650
- Speck, A. K., Hofmeister, A. M., & Barlow, M. J. 1999, *ApJ*, 513, L87
- Tanner, A., et al. 2002, *ApJ*, 575, 860
- Tielens, A. G. G. M. 1998, *ApJ*, 499, 267
- Tielens, A. G. G. M., Wooden, D. H., Allamandola, L. J., Bregman, J., & Witteborn, F. C. 1996, *ApJ*, 461, 210
- Todini, P., & Ferrara, A. 2001, *MNRAS*, 325, 726
- Vriend, W. J. 1999, M.S. thesis, Groningen Univ.
- Waelkens, C., et al. 1996, *A&A*, 315, L245
- Wang, S. X., Wang, L. M., Ewing, R. C., & Doremus, R. H. 1998, *J. Non-Cryst. Solids*, 238, 198
- Waters, L. B. F. M., Molster, F. J., de Jong, T., et al. 1996, *A&A*, 315, L361
- Wefel, J. P. 1988, in *Genesis and Propagation of Cosmic Rays*, ed. M. M. Shapiro & J. P. Wefel (Dordrecht: Reidel), 1
- Whittet, D. C. B. 2003, *Dust in the Galactic Environment* (2nd ed.; London: IoP)
- Whittet, D. C. B., Duley, W. W., & Martin, P. G. 1990, *MNRAS*, 244, 427
- Witt, A. N., Smith, R. K., & Dwek, E. 2001, *ApJ*, 550, L201
- Wooden, D. H. 2002, *Earth Moon Planets*, 89, 247